# Epstein–Barr Virus–Encoded Circular RNA CircBART2.2 Promotes Immune Escape of Nasopharyngeal Carcinoma by Regulating PD-L1

Junshang Ge[1,2], Jie Wang[1,2], Fang Xiong[3], Xianjie Jiang[1,2], Kunjie Zhu[1], Yian Wang[1,2], Yongzhen Mo[1,2], Zhaojian Gong[4], Shanshan Zhang[3], Yi He[1], Xiayu Li[5], Lei Shi[2,4], Can Guo[1,2], Fuyan Wang[2], Ming Zhou[1,2], Bo Xiang[1,2], Yong Li[6], Guiyuan Li[1,2], Wei Xiong[1,2], and Zhaoyang Zeng[1,2]

## ABSTRACT

Epstein–Barr virus (EBV) infection is an established cause of nasopharyngeal carcinoma (NPC) and is involved in a variety of malignant phenotypes, including tumor immune escape. EBV can encode a variety of circular RNAs (circRNA), however, little is known regarding the biological functions of these circRNAs in NPC. In this study, EBV-encoded *circBART2.2* was found to be highly expressed in NPC where it upregulated PD-L1 expression and inhibited T-cell function *in vitro* and *in vivo*. *circBART2.2* promoted transcription of PD-L1 by binding the helicase domain of RIG-I and activating transcription factors IRF3 and NF-κB, resulting in tumor immune escape. These results elucidate the biological function of *circBART2.2*, explain a novel mechanism of immune escape caused by EBV infection, and provide a new immunotherapy target for treating NPC.

**Significance:** This work demonstrates that *circBART2.2* binding to RIG-I is essential for the regulation of PD-L1 and subsequent immune escape in nasopharyngeal carcinoma.

## Introduction

The programmed cell death-1/programmed cell death-ligand 1 (PD-1/PD-L1) signaling pathway is an important mechanism mediating tumor immunosuppression (1). PD-L1 is often expressed on the surface of tumor cells and immunosuppressive cells in the tumor microenvironment and interacts with PD-1 on T cells. This immune checkpoint prevents tumor antigen–specific T cells from being effectively activated and killing tumor cells, resulting in tumor immune escape. Based on this mechanism, antibodies targeting PD-1 and PD-L1 protein have been rapidly developed for the treatment of cancer, with some showing remarkable curative effects in immune-related tumors (2). However, the accumulated data from clinical trials for solid tumors revealed that the antitumor response rate of PD-1 inhibitors is not significantly high (3–6). Therefore, it is urgent to clarify the mechanisms regulating PD-1/PD-L1 expression in cancer.

Nasopharyngeal carcinoma (NPC) is a type of malignant tumor that originates in the nasopharyngeal epithelium, with distinct ethnic and regional differences in its incidence and common malignant tumors in South China and Southeast Asia (7, 8). Genetic susceptibility and environmental factors [including Epstein–Barr virus (EBV) infection] are the leading causes of NPC (9–11). EBV infects more than 95% of adults worldwide (12, 13) and is associated many kinds of tumors including NPC and gastric cancer (14). EBV infection is involved in NPC proliferation, migration, invasion, and tumor immune escape, through EBV-encoded proteins or noncoding RNAs such as microRNAs (miRNA) and long noncoding RNAs (15, 16). EBV can also encode various circular RNAs (circRNA), which are noncoding RNAs with a circular structure (17). Toptan and colleagues first reported that three gene loci (*BART, LMP2*, and *BHLF1*) encode circRNAs in EBV (17). *LMP2* and *BHLF1* genes can encode *circLMP2* and *circBHLF1*, whereas the *BART* gene has abundant variable splicing sites and can encode four different circBARTs, namely, *circBART1.1* (711 nt, including exons II, IIIa, IIIb, IV, and intron IIIa), *circBART1.2* (509 nt, including exons II, IIIa, IIIb, and IV), *circBART2.1* (609 nt, including exons IIIa, IIIb, IV, and intron IIIa), and *circBART2.2* (399 nt, including exons IIIa, IIIb, and IV). However, the functions of these circRNAs in NPC remain unclear (18, 19).

circRNAs are a class of ncRNAs characterized by a covalent closed-loop structure without 5- or 3-ends and not easily degraded by exonucleases (20). Several circRNAs are reported to dysregulate in different types of cancers and function as competitive endogenous RNAs (ceRNA), protein-binding or protein-coding RNAs to regulate the gene expression and are involved in tumorigenesis and progression (21, 22). In NPC, multiple circRNAs participate in the regulation of tumor cell biological functions through the ceRNA mechanism, including *circARHGAP12* (23), *circSETD3* (24), or even EBV-encoded

[1]NHC Key Laboratory of Carcinogenesis and Hunan Key Laboratory of Cancer Metabolism, Hunan Cancer Hospital and the Affiliated Cancer Hospital of Xiangya School of Medicine, Central South University, Changsha, Hunan, China. [2]Key Laboratory of Carcinogenesis and Cancer Invasion of the Chinese Ministry of Education, Cancer Research Institute and School of Basic Medicine Sciences, Central South University, Changsha, Hunan, China. [3]Department of Stomatology, Xiangya Hospital, Central South University, Changsha, Hunan, China. [4]Department of Oral and Maxillofacial Surgery, The Second Xiangya Hospital, Central South University, Changsha, Hunan, China. [5]Hunan Key Laboratory of Nonresolving Inflammation and Cancer, Disease Genome Research Center, The Third Xiangya Hospital, Central South University, Changsha, Hunan, China. [6]Department of Medicine, Dan L Duncan Comprehensive Cancer Center, Baylor College of Medicine, Houston, Texas.

**Note:** Supplementary data for this article are available at Cancer Research Online (http://cancerres.aacrjournals.org/).

**Corresponding Author:** Zhaoyang Zeng, Hunan Cancer Hospital and the Affiliated Cancer Hospital of Xiangya School of Medicine, Central South University, Changsha, Hunan 410013, China. Phone: 86-731-84805446; E-mail: zengzhaoyang@csu.edu.cn

Cancer Res 2021;81:5074–88

**doi:** 10.1158/0008-5472.CAN-20-4321

*circRPMS1* (also *circBART2.2*; refs. 25–27). However, the mechanism of circRNAs reported in NPC mainly focuses on tumor malignant biological properties. Further insight into the role of circRNAs in tumor immune escape may contribute to understanding the development of NPC.

RIG-I (retinoic acid-inducible gene I) is a cytoplasmic sensor of double-stranded RNA due to the unique structural combination of an N-terminal caspase recruitment domain (CARD) and a C-terminal DExD/H RNA helicase domain. It plays an important role in the host defense response to eliminate invading viruses. It has been reported that EBV-encoded RNA *EBERs*, LMP1, and EBV-encoded *miR-BART6-3p* are recognized by RIG-I (28–30) and evade immune surveillance.

In this study, we assessed the function of EBV-encoded *circBART2.2* in NPC and found that RIG-I through its helicase domain recognized the nucleotides from 114–165 bp of *circBART2.2*, which promoted PD-L1 expression through activating canonical transcription factors including interferon regulator factor 3 and NF-κB in NPC, resulting in tumor immune escape. The role of *circBART2.2*–RIG-I interaction in triggering tumor immune escape through the PD-1 immune-checkpoint pathway may shed light on NPC treatment, which will provide new therapeutic targets focusing on *circBART2.2*-activated tumor immunotherapy.

## Materials and Methods

### Patient samples

A total of 72 NPC and 20 nontumor nasopharyngeal epithelial tissues from patients with chronic nasopharyngeal inflammation (Supplementary Table S1) were collected for quantitative RT-PCR. And 52 NPC and 36 noncancerous nasopharyngeal epithelial tissue samples from patients with chronic nasopharyngeal inflammation or the adjacency of NPC tissues were collected for *in situ* hybridization or IHC (Supplementary Table S2). All the clinical samples were approved by the Research Ethics Committee of the Second Xiangya Hospital, Central South University according to the ethical and legal standards Declaration of Helsinki. The patients were provided with the informed written consent before surgery.

### Cell lines, reagents, plasmids, and cell transfection

EBV-uninfected (HONE1 and HK1) and -infected (HONE1-EBV and HK1-EBV) NPC cell lines, and EBV-positive NPC cell line C666-1 (RRID: CVCL_7949) were gifted by Professor George Sai Wah Tsao, University of Hong Kong and Professor Xin Li, Southern Medical University (31). EBV-negative Akata and EBV-positive Akata were cultured and amplified in RPMI-1640 medium in our laboratory, which was supplemented with 10% fetal bovine serum (Invitrogen), penicillin (100 U/mL, Sigma-Aldrich), and streptomycin (100 U/mL, Sigma-Aldrich). All cells were confirmed to be *Mycoplasma* negative before culture (TaKaRa) and were authenticated by the STR Multi-amplification Kit (Goldeneye- DNA ID system 20A, Peoplespot) every six months. The length of time between thawing and use is less than 3 months.

Prediction of the secondary stem loop structure of *circBART2.2* was performed using the RNAfold database (http://rna.tbi.univie.ac.at/), and three well-characterized stem loop structures were selected for deletion mutants. Full-length *circBART2.2* and deletion mutants were cloned into pcDNA3.1$^{+}$ circRNA mini vectors containing tandem repeat sequences at both ends of the inserted sequence to aid circRNA looping, followed by Sanger sequencing. Prediction of the RIG-I function domain was performed using the UniProt database (https://www.uniprot.org/, Universal Protein Resource, RRID: SCR_002380). Additionally, flag-tagged full-length RIG-I and its truncations were synthesized and cloned into the pcDNA3.1 vector (Invitrogen, RRID: Addgene_79663).

The nontarget scrambled siRNA controls were provided by GenePharma. Three siRNAs specifically targeting the splice site of *circBART2.2* were also synthesized and transfected into HONE1-EBV and HK1-EBV. Two siRNAs of RIG-I were used to knockdown of RIG-I. Lipofectamine RNAiMAX Reagent (Invitrogen) with OptiMEM medium (Invitrogen) was used for transfection.

For RNase R (RNR07250, Epicentre) treatment, total RNA were incubated with RNase R (20 U/μL) at 37°C for 30 minutes and at 70°C for 10 minutes to inactivation and then for quantitative real-time PCR (qRT-PCR) detection.

For actinomycin D (A4262, Sigma) treatment, cells were treated with actinomycin D (1 μg/mL) for 0, 6, 12, and 24 hours and then for qRT-PCR detection.

For treatment with anti–PD-L1 antibody, sufficient anti–PD-L1 antibody (5 mg/mL, atezolizumab, AbMole) was added and cocultured for 3 hours with activated primary T cells.

### Quantitative real-time PCR and regular PCR

Total RNA was extracted using TRIzol reagent (15596026, Invitrogen) and reverse transcribed using the HiScript cDNA Synthesis kit (R323-01, Vazyme). qRT-PCR was performed using the Universal SYBR qPCR Master Mix (Q511-02, Vazyme). The $2^{-\Delta\Delta C_t}$ method was used to normalize the data.

Regular PCR experiments were carried out using the Golden Star T6 Super PCR Mix (TSE101, Tsingke) according to the instructions. Primers are listed in Supplementary Table S3. To amplify four different circBART variants, isoform-specific primers that could be discriminated each other were designed (**Fig. 1A**). The primers for *circBART2.2* were designed according to its circular splice site spanning exons IV and IIIA of the *BART* gene, which were specific to *circBART2.2* and the linear forms could not be detected. *circBART2.1* and *circBART2.2* could also be discriminated.

### Immunofluorescence and fluorescence *in situ* hybridization

Immunofluorescence was performed according to the manufacturer's instructions. Images were captured using the Operetta CLS High-Content Fluorescence Analysis System (PerkinElmer).

The digoxigenin-labeled specific probe for *circBART2.2* was designed and synthesized by Tsingke Co. The fluorescence *in situ* hybridization (FISH) experiment was performed according to the manufacturer's instructions (RiboBio). The nuclei were counterstained with 4′, 6-diamidino-2-phenylindole (DAPI; D1306, Invitrogen). Cells were imaged using a confocal laser scanning microscope (PerkinElmer).

### Western blotting

The total protein was extracted and separated by 10% twelve alkyl sulfate polyacrylamide gel electrophoresis (SDS-PAGE) and then transferred to polyvinylidene fluoride membrane (IEVH07850, Millipore). The membrane was incubated antibodies, and the ECL detection reagent (Millipore) was used to detect. GAPDH was used as a protein control. Antibodies are shown in Supplementary Table S4.

### IHC and *in situ* hybridization

IHC was performed using the Elivision plus Polyer HRP (Mouse/Rabbit) IHC Kit (KIT-9902, Maxim), and the primary antibodies used are shown in Supplementary Table S4.

*In situ* hybridization was performed using the Enhanced Sensitive ISH Detection kit I (POD; MK1030, BOSTER, China) kit using the

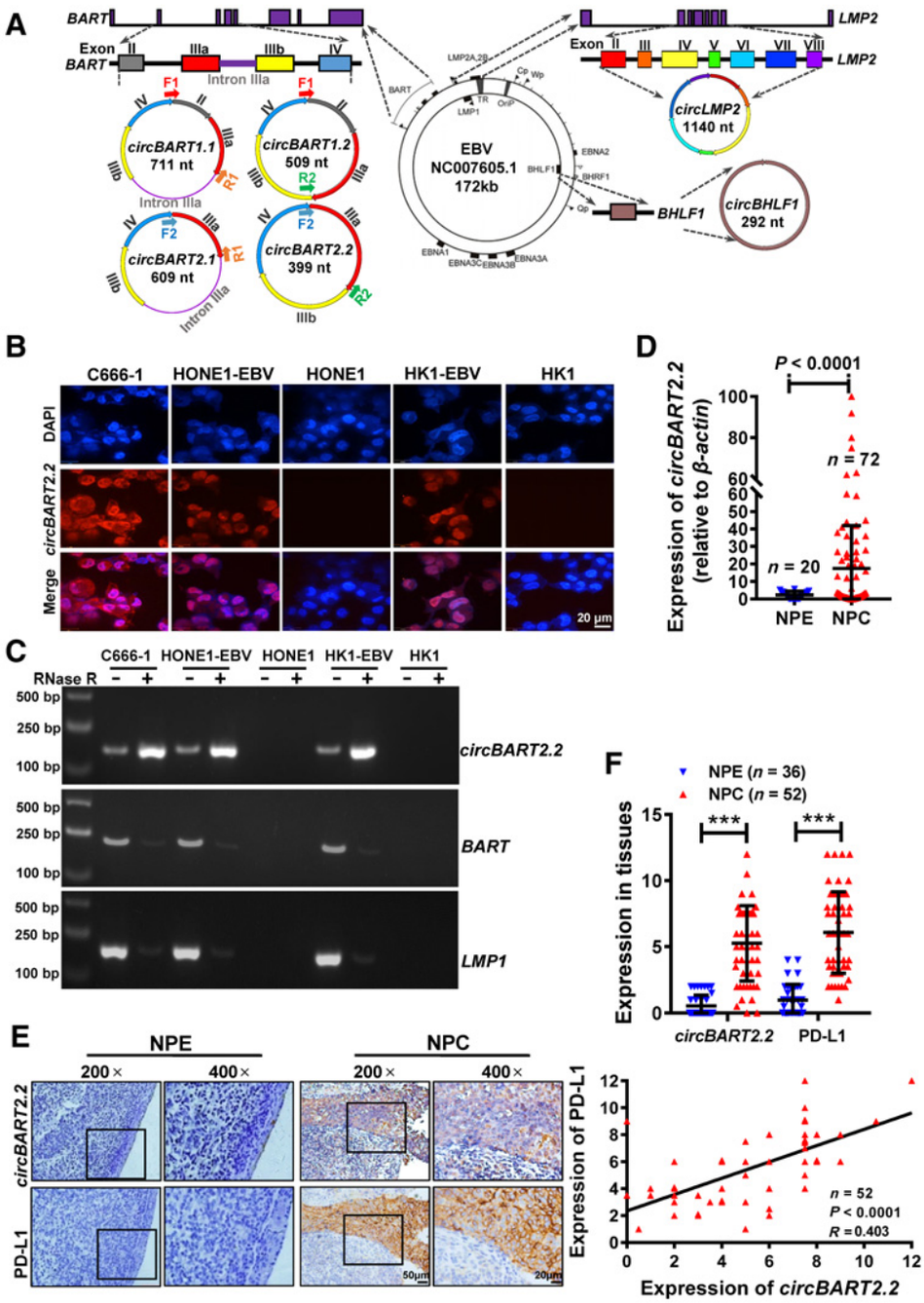


**Figure 1.**

EBV-encoded *circBART2.2* was highly expressed in NPC and positively correlated with PD-L1. **A,** Schematic diagram of EBV-encoded circRNAs in EBV (NC007605.1, 172 kb). The *LMP2* gene encodes *circLMP2* (1140 nt), and *BHLF1* encodes *circBHLF1* (292 nt). The *BART* gene encodes four different circBARTs: *circBART1.1* (711 nt, including exons II, IIIa, IIIb, and IV and intron IIIa), *circBART1.2* (509 nt, including exons II, IIIa, IIIb, and IV), *circBART2.1* (609 nt, including exons IIIa, IIIb, and IV and intron IIIa), and *circBART2.2* (399 nt, including exons IIIa, IIIb, and IV). F1, F2, R1, and R2: primer sites for detecting circBARTs are indicated. **B,** Intracellular localization of *circBART2.2* (red) in the EBV-positive NPC cell lines C666-1, HONE1-EBV, and HK1-EBV, as determined by FISH using a biotin-labeled *circBART2.2* probe. EBV-negative HONE1 and HK1 were used as the negative controls. Nuclei were stained with DAPI (blue). Magnification, ×400. Scale bar, 20 μm. **C,** The stability of *circBART2.2* was detected in RNase R–treated C666-1, HONE1-EBV, and HK1-EBV cells for 24 hours by qPCR. EBV-negative HONE1 and HK1 were used as negative controls. The linear *BART* and *LMP2* mRNA were also used as controls. **D,** *circBART2.2* expression was measured in 72 NPC tissues and 20 noncancerous nasopharyngeal epithelial (NPE) tissue samples by RT-PCR. *β-Actin* was used as an internal reference ($P < 0.0001$). **E,** Representative images of *circBART2.2* and PD-L1 expression in 52 NPC tissues and 36 noncancerous NPE tissues by *in situ* hybridization for *circBART2.2* and IHC for PD-L1 protein. Magnification, ×200; scale bar, 50 μm; ×400; scale bar, 20 μm. **F,** Statistical analysis of the expression and correlation of *circBART2.2* and PD-L1 according to the expression in 52 NPC tissues and 36 noncancerous NPE tissue samples by *in situ* hybridization or IHC. ***, $P < 0.001$.

digoxigenin-labeled *circBART2.2* probe (Tsingke) according to the manufacturer's instructions. The staining intensity score was determined as 0 = negative, 1 = weak, 2 = moderate, and 3 = strong, and the positive rate score was determined as 0 = negative, 1 = 1%–25%, 2 = 26%–50%, 3 = 51%–75%, and 4 = 76%–100%. The total score was obtained by multiplying the intensity and positive rate scores of the stained cells and completed by two experienced pathologists. Images were captured using an Olympus BX51 fluorescence microscope (Olympus).

### Enzyme linked immunosorbent assay

The concentration of IFNγ in serum of nude mice or CD8-positive T cells was measured by the IFNγ ELISA Kit (KHC4021, eBioscience) according to the manufacturer's guidelines.

### Flow cytometry analysis

An Annexin V–FITC Apoptosis Detection Kit (BMS500FI, Invitrogen) was used to detect apoptosis by flow-cytometric analysis. Cells were incubated with Alexa Fluor 488 Annexin V and propidium iodide (PI) for 15 minutes and performed using the DX athenatm flow cytometry. The FlowJo software (FlowJo, RRID: SCR_008520) was used for data analysis. Unstained cells and fluorescence minus controls were used for cytometry and gating set up. Q1: Annexin $V^-/PI^+$, Q2: Annexin $V^+/PI^+$, Q3: Annexin $V^-/PI^-$, Q4: Annexin $V^+/PI^-$.

### RNA pulldown and liquid chromatography coupled to tandem mass spectrometry

An RNA pulldown assay was performed using a magnetic RNA protein pulldown kit (20164, Thermo Scientific) according to the manufacturer's instructions. In short, biotin-labeled specific *circBART2.2* probe or its fragments (367–11 nt for DEL1, 114–165 nt for DEL2, and 62–89 nt for DEL3) that deleted the core structural area of *circBART2.2* were designed. The *circBART2.2* or its fragment overexpression vectors were transfected into cells. After 24 hours, the biotin-labeled or unbiotin-labeled probes were transfected into cells for another 24 hours. The cell lysates were incubated with biotin-affinity magnetic beads for 2 hours at room temperature to bind the RNA-associated proteins. The purified proteins were separated using SDS-PAGE gels and then stained with Coomassie blue staining and analyzed by liquid chromatography coupled to tandem mass spectrometry (LC-MS/MS) using an UltiMate 3000 RSLCnano system coupled to an LTQ OrbitrapVelos Pro mass spectrometer (Thermo Scientific).

### RNA immunoprecipitation analysis

Cells were incubated with anti-RIG-I or rabbit IgG control-coupled magnetic beads. RNA in immunoprecipitates was isolated with TRIzol reagent and analyzed by qRT-PCR.

### Luciferase reporter analysis

Vectors for the reporter genes detecting the ISRE and NF-κB activities were purchased from Beyotime Biotechnology (pISRE-TA-luc, D2179, pNF-κB-luc, and D2206). For the PD-L1 promoter analysis, different lengths of the PD-L1 promoter and corresponding mutant fragments were cloned into the PGL3 basic vector (E1751, Promega). The ratio of the luminescence of the firefly luciferase to that of the *Renilla* luciferase was calculated using the Dual-Glo Luciferase Assay System (E2980, Promega) kit.

### Chromatin immunoprecipitation

Chromatin immunoprecipitation (ChIP) analysis was performed using the Pierce Magnetic ChIP Kit (26157, Thermo Scientific). The NF-κB (p65) and IRF3 antibodies were used to enrich the *PD-L1* promoter region fragments, and then qPCR was used to analyze the expression of the enriched fragments.

### Preparation of dendritic cells and primary T cells

After testing, HONE1 was classified as HLA-$A2^+$. The peripheral blood of HLA-$A2^+$ healthy donors was used to prepare dendritic cells. First, peripheral blood mononuclear cell was separated using the Ficoll (45-001-749, Cytiva) separation solution and added to 10% FBS-1640 medium containing 50 ng/m LGM-CSF (PHC2013, Invitrogen) and 20 ng/mL IL4 (PHC0044, Invitrogen) for 5 days. To promote the maturation of dendritic cells, 25 ng/mL IFNγ (Invitrogen) was added and cultured for 1 day, and then cocultured with HONE1 lysate for another day. To expand T cells *in vitro*, T cells were added with CD3/CD28 amplified magnetic beads (Miltenyi Biotec) and 15 ng/mL IL2 (PHC0026, Invitrogen), 5 ng/mL IL7 (PHC0073, Invitrogen), and 10 mL IL15 (PHC9151, Invitrogen) for 8-day culture. To generate tumor-specific cytotoxic T-lymphocytes, the prepared dendritic cells and expanded T cells were cocultured in a medium supplemented with IL2, IL7, and IL15 for 5 days at a ratio of 1:5.

### Real-time tracking T-cell activity status using the high-content cell imaging analysis system

HONE1 cells stained with the CellTracker CM-DiI Dye (C7000, Invitrogen) and activated human primary T cells labeled with live-cell fluorescent dye CMFDA (5-chloromethylfluorescein diacetate, C7025, Invitrogen) at the ratio of 1: 10 were cocultured for 3 hours. The Operetta CLS high-content cell imaging analysis system (PerkinElmer) was used to track the fluorescence status of T cells in real time.

### Nude mouse model *in vivo*

HONE1 cells ($5 \times 10^6$) transfected with the *circBART2.2* overexpression vector or the empty vector were injected subcutaneously into the right thigh root of 4 weeks old and female nude mice (22 mice per group). Tumor formation was observed macroscopically 7 days later. Dendritic cells were first cocultured with HONE1 cell lysate for 24 hours, and then cocultured with T cells to present HONE1-specific tumor antigens to T cells to enable them to produce HONE1-specific T cells. For one part, human primary T cells that had received tumor-specific antigen presentation were labeled with Deep Red live-cell fluorescent dye (DiR, Thermo Fisher) and injected into the mice through the tail vein (3 mice per group) to evaluate T cells distribution in nude mice using the small animal *in vivo* imaging system (Bruker).

For the second part, T cells that had received tumor-specific antigen presentation without Deep Red live-cell fluorescent dye were injected into the mice (5 mice per group) to evaluate T cells survival. The mice peripheral blood was extracted for qRT-PCR, ELISA, or flow-cytometric analysis after 7 days of adoptive T cells treatment.

For the third part, T cells without fluorescent dye were also injected into nude mice (7 mice per group) for 32 days. Tumor volume, size, weight, and body weight of nude mice were measured. *In situ* hybridization or IHC were performed to examine the expression of *circBART2.2*, RIG-I, PD-L1, cleaved caspase-3, and cleaved-PARP. All animal studies were approved by the Ethics Committee of the Xiangya Hospital, Central South University.

### Data analysis and statistical analysis

The NPC gene-expression data set (GSE12452) was downloaded from the Gene-Expression Omnibus (GEO, RRID: SCR_005012) database. Statistical analysis was performed using the GraphPad Prism

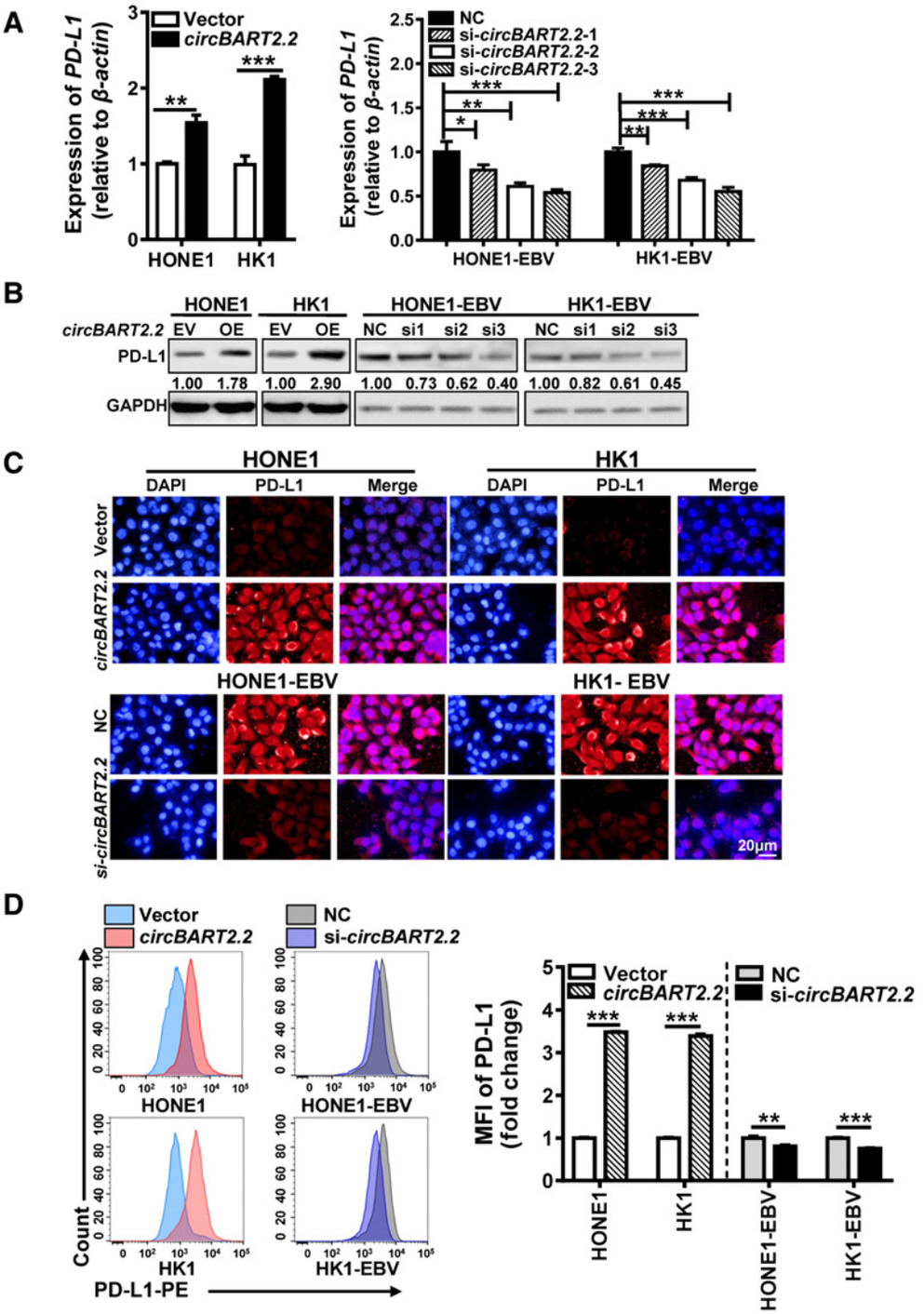


**Figure 2.**

*circBART2.2* significantly upregulated PD-L1 expression. **A,** The mRNA expression of PD-L1 was examined in HONE1 and HK1 cells after *circBART2.2* overexpression or in HONE1-EBV and HK1-EBV cells transfected with three *circBART2.2* siRNAs, respectively, as demonstrated by RT-PCR. *, $P < 0.05$; **, $P < 0.01$; ***, $P < 0.001$. **B,** The expression of PD-L1 protein was examined in HONE1 and HK1 cells after *circBART2.2* overexpression or in HONE1-EBV and HK1-EBV cells transfected with three *circBART2.2* siRNAs, respectively, as demonstrated by Western blotting. **C,** PD-L1 expression (red) was measured in EBV-negative or -positive NPC cells after *circBART2.2* overexpression or knockdown by immunofluorescence using anti–PD-L1 antibody. Nuclei were stained with DAPI (blue). Magnification, ×400. Scale bar, 20 μm. **D,** PD-L1 expression was measured in EBV-negative or -positive NPC cells after *circBART2.2* overexpression or knockdown using flow-cytometric analysis using APC-stained anti–PD-L1 antibody. Left, original flow cytometry results; right, statistical results. Three independent replicates were evaluated for each group. MFI: mean fluorescence intensity. **, $P < 0.01$; ***, $P < 0.001$.

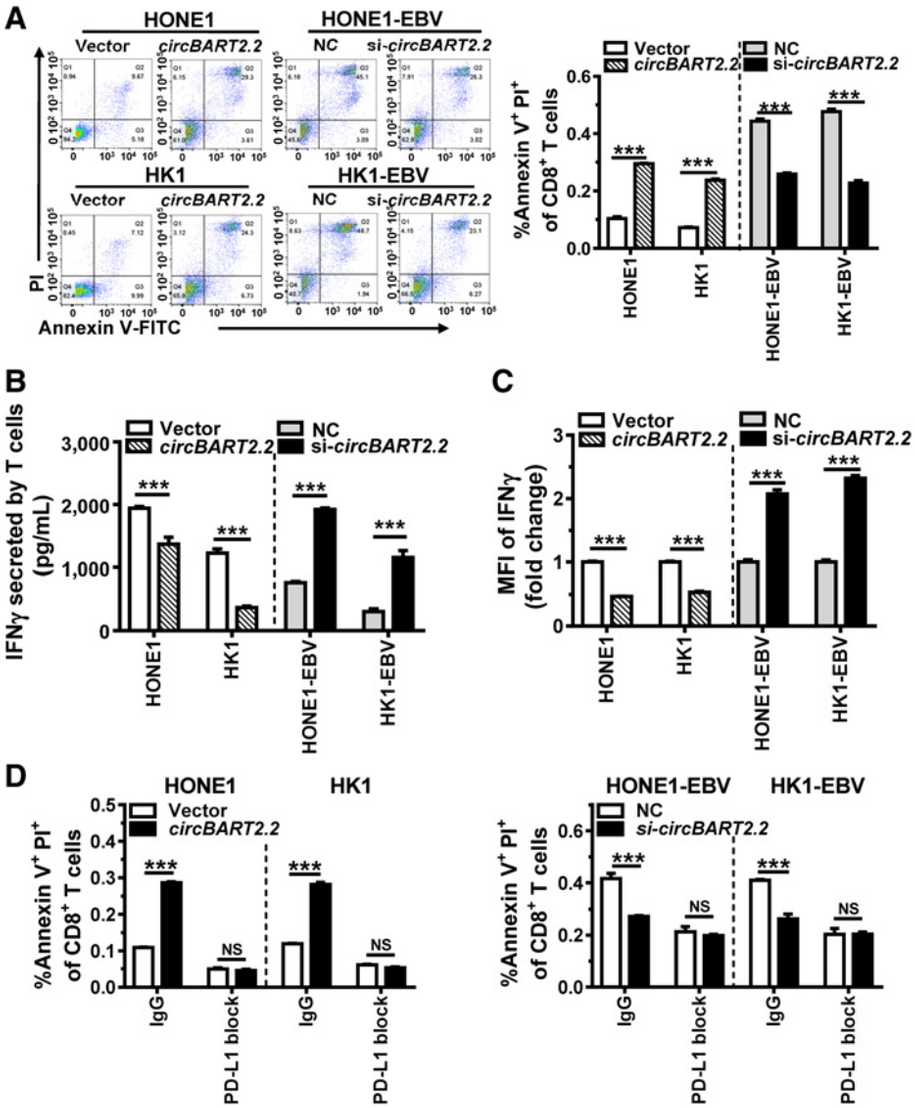


**Figure 3.**

*circBART2.2* promoted T-cell apoptosis and inhibited IFNγ secretion of T cells through PD-L1. **A,** The degree of T-cell apoptosis was measured by flow cytometry in EBV-negative or -positive NPC cells after *circBART2.2* overexpression or knockdown after incubation with Alexa Fluor 488 Annexin V and PI. Left, original flow cytometry results; right, statistical results. ***, $P < 0.001$. Q1, Annexin $V^-/PI^+$; Q2, Annexin $V^+PI^+$; Q3, Annexin $V^-/PI^-$; Q4, Annexin $V^+/PI^-$. **B,** IFNγ secretion from T cells was measured by ELISA in EBV-negative or -positive NPC cells after *circBART2.2* overexpression or knockdown. ***, $P < 0.001$. **C,** The concentration of IFNγ in cell culture medium was examined by flow-cytometric analysis in T cells cocultured with EBV-negative or -positive NPC cells after *circBART2.2* overexpression or knockdown using APC-stained anti-IFNγ antibody. Each experiment was independently repeated three times, and the original results are shown in Supplementary Fig. S4A. MFI, mean fluorescence intensity; ***, $P < 0.001$. **D,** Annexin $V^+$ $PI^+$ cells of CD8-positive active T cells were measured by flow cytometry in T cells cocultured with EBV-negative or -positive NPC cells after *circBART2.2* overexpression or knockdown. NPC cells were treated with a sufficient anti–PD-L1 antibody to block PD-L1 activity. Each experiment was independently repeated three times, and the original results are shown in Supplementary Fig. S4B. NS, not significant; ***, $P < 0.001$.

7.0 (GraphPad Prism, Inc.; RRID: SCR_002798). Two-tailed *t* tests were used to analyze the data. *P* values < 0.05 were considered statistically significant.

### Availability of data and materials

All data that support the findings of this study are available from the corresponding authors upon reasonable request.

## Results

### EBV-encoded circBART2.2 was highly expressed and positively correlated with PD-L1 expression in NPC

To identify the role of EBV-encoded circRNAs in the development of NPC, qRT-PCR was performed in six EBV-positive NPC clinical samples and EBV-positive cell lines. Isoform-specific primers that could be discriminated from each other were designed for circRNAs. For four circBART variants, the forward primer was overlapped with the back splice sequence (either backsplice of exon IV to II for 1.1 and 1.2 variants or backsplice of exon IV to IIIa for 2.1 and 2.2) variants and the reverse primers overlapped the exon-exon junctions exon IIIb to IIIa (for variants 1.2 and 2.2) or Intron IIIa to exon IIIa (for variants 1.1 and 2.1; **Fig. 1A**). All four different variants were discriminated and expressed in the EBV-positive Akata cell line, which was consistent with Toptan and colleagues (17). *circBART2.2* was detected at high levels in all six NPC clinical tissues and EBV-positive NPC cell lines, including C666-1, HONE1-EBV, and HK1-EBV. *circBART2.1* was weakly detected in C666-1, HONE1-EBV, and HK1-EBV, but was not expressed in six NPC tissues. *circBART1.1, circBART1.2, circLMP2*, and *circBHLF1* were only detected in Akata; additionally, there were no specific electrophoretic bands in six NPC clinical samples and other EBV-positive NPC cells (Supplementary Fig. S1A). These data suggest that *circBART2.2* may be expressed in EBV-positive NPC with the high levels, thereby affecting the development of NPC.

Using RNA FISH (**Fig. 1B**), the expression of *circBART2.2* was detected in C666-1, HONE1-EBV, and HK1-EBV, but not in HONE1 and HK1. *circBART2.2* was resistant to RNase R degradation and more stable than linear *BART* mRNA in C666-1, HONE1-EBV, and HK1-

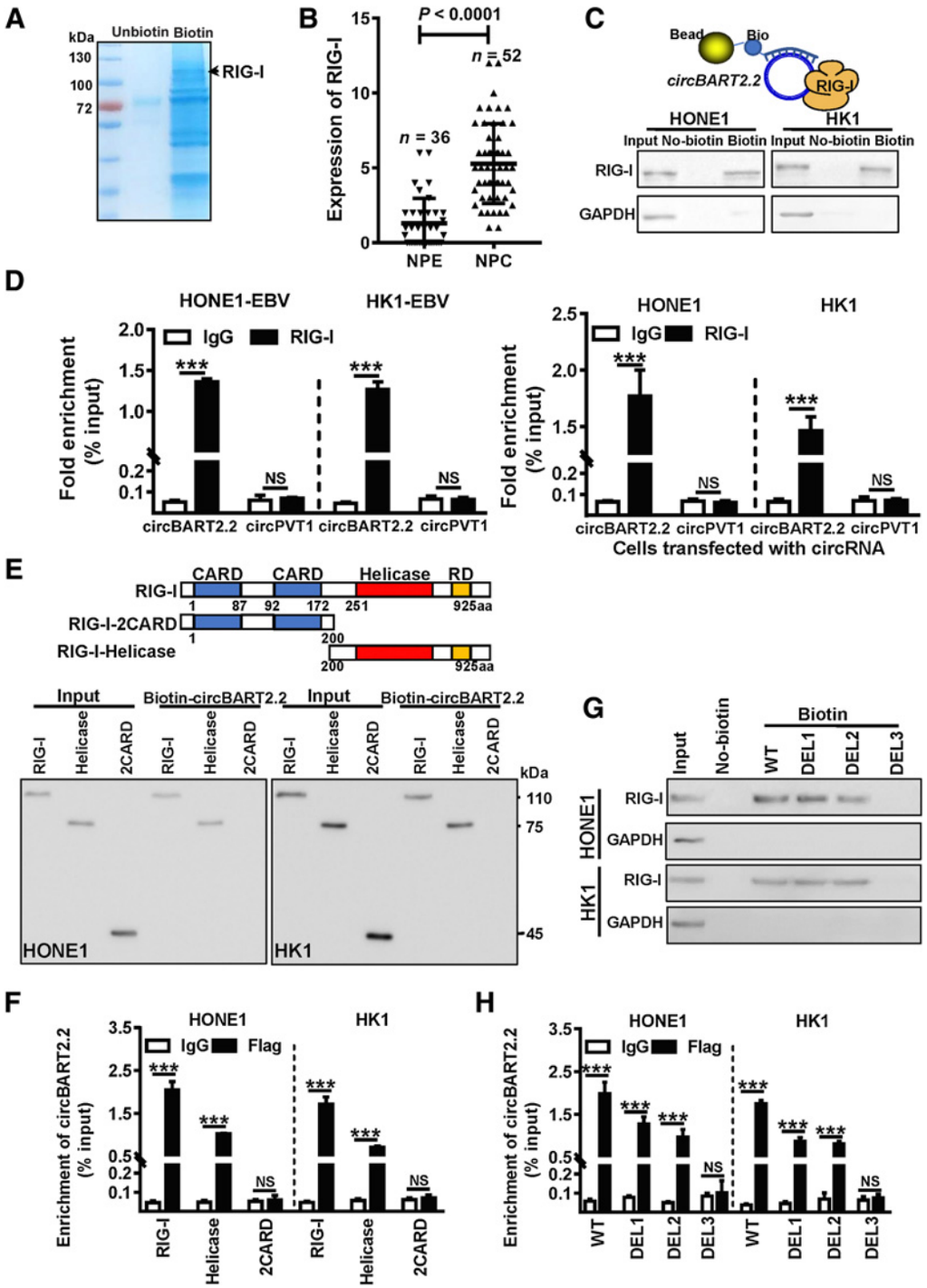


**Figure 4.**

*circBART2.2* binds to RIG-I protein through the helicase domain. **A,** Biotin-labeled or unbiotin-labeled *circBART2.2* probes were transfected into HONE1 cells after the overexpression of *circBART2.2*. The cell lysates were incubated with biotin-affinity magnetic beads for 2 hours. The precipitated proteins were resolved by SDS-PAGE, followed by Coomassie blue staining. Next, the differential band in the biotin-labeled *circBART2.2* probe lane was identified by LC-MS/MS. The unbiotin-labeled *circBART2.2* probe served as a control. RIG-I was also identified. **B,** The expression of RIG-I in 52 NPC tissues and 36 noncancerous NPE tissues by IHC using an anti-RIG-I antibody. $P < 0.0001$. **C,** Binding of *circBART2.2* to RIG-I protein was detected in HONE1 and HK1 cells after overexpression of *circBART2.2* using RNA pulldown assays with a biotin-labeled *circBART2.2* probe. The unbiotin-labeled *circBART2.2* probe was used for control. **D,** Direct binding of RIG-I protein to *circBART2.2* was evaluated in HONE1 and HK1 cells after overexpression of *circBART2.2* or in EBV-positive HONE1-EBV and HK1-EBV cells by RNA immunoprecipitation using anti–RIG-I antibody, followed by qPCR analysis for *circBART2.2*. *CircPVT1* was used as a negative control. (*Continued on the following page.*)

EBV after RNase R (**Fig. 1C**) or actinomycin D treatments (Supplementary Fig. S1B). Additionally, high expression of *circBART2.2* was confirmed in 72 NPC tissues and 20 nasopharyngeal epithelial tissues by qRT-PCR (**Fig. 1D**) and in 52 NPC and 36 noncancerous samples by *in situ* hybridization (**Fig. 1E** and **F**).

To examine whether *circBART2.2* is involved in the PD-L1–regulated immune escape in NPC, we analyzed the correlation between *circBART2.2* and PD-L1. PD-L1 was highly expressed in the same NPC tissues by IHC and significantly positively correlated with the expression of *circBART2.2* (**Fig. 1E** and **F**).

## circBART2.2 inhibited T-cell killing of NPC cells by upregulating PD-L1

To further validate the correlation between *circBART2.2* and PD-L1 in NPC, a *circBART2.2* overexpression vector was transfected into HONE1 and HK1 (Supplementary Fig. S2A). The expression of *circBART2.2* was stable and resistant to RNase R degradation after overexpression of *circBART2.2* in HONE1 and HK1, compared with *GAPDH* mRNA (Supplementary Fig. S2B). Additionally, three siRNAs specifically targeting the splice site of *circBART2.2* were transfected into HONE1-EBV and HK1-EBV, and knockdown of *circBART2.2* (Supplementary Fig. S2C) reduced *circBART2.2* expression, but not linear *BART*. siRNAs targeting *circBART2.2* also had some effect on the *circBART2.1* expression because they shared the same back splice site. However, compared with *circBART2.2*, the expression of *circBART2.1* in HONE1-EBV and HK1-EBV was extremely low (Supplementary Fig. S2C). In contrast, PD-L1 expression is not affected by *circBART2.1* overexpression in HONE1 and HK1 cells (Supplementary Fig. S2D). We speculate that *circBART2.1* may have little influence on the regulation of PD-L1 in NPC.

RT-PCR and Western blotting showed that overexpression of *circBART2.2* promoted PD-L1 expression at the mRNA (**Fig. 2A**) and protein levels (**Fig. 2B**), while PD-L1 expression was diminished after *circBART2.2* siRNA treatment. Immunofluorescence (**Fig. 2C**) and flow cytometry (**Fig. 2D**) using anti–PD-L1 antibody also showed that *circBART2.2* promoted PD-L1 expression. In summary, *circBART2.2* is a potent inducer of PD-L1 in EBV-associated NPC.

To determine whether *circBART2.2* inhibits T-cell function and mediates NPC immune escape through PD-L1, *circBART2.2* was overexpressed or knocked down in NPC cells. Then cells were stained with DeepRed live-cell fluorescent dye and cocultured with activated primary cultured T cells labeled with the live-cell fluorescent dye CMFDA. The T-cell viability status was tracked in real time using a high-content cell imaging analysis system (Supplementary Fig. S3A). The fluorescence intensity of T cells decreased faster than that of control cells in NPC cells when *circBART2.2* was overexpressed, whereas knockdown of *circBART2.2* in EBV-infected NPC cells inhibited the decrease of T cells' fluorescence intensity, suggesting *circBART2.2* effectively promoted T-cell apoptosis in NPC. By contrast, the fluorescence intensity of NPC cells decreased in a slower manner than that of control cells after overexpression of *circBART2.2* by flow cytometry (Supplementary Fig. S3B), suggesting that *circBART2.2* promoted the immune escape of NPC cells.

$CD8^+$ T cells can be used to measure the activity of T cells. Flow cytometry using anti-CD8 antibody showed that T-cell apoptosis (Annexin $V^+PI^+$) in coculture with NPC cells was significantly increased after overexpression of *circBART2.2* and significantly decreased after knockdown of *circBART2.2* (**Fig. 3A**). Cytotoxic T cells inhibit tumor growth through IFNγ secretion. Overexpression of *circBART2.2* in NPC cells significantly inhibited IFNγ secretion of T cells, and knockdown of *circBART2.2* restored the ability of T cells to secrete IFNγ (**Fig. 3B**). Flow cytometry using anti-IFNγ antibody showed that overexpression of *circBART2.2* significantly inhibited IFNγ accumulation in T cells, whereas knockdown of *circBART2.2* partially restored the ability of T cells to produce IFNγ (**Fig. 3C**; Supplementary Fig. S3C). Notably, a sufficient anti–PD-L1 antibody to block PD-L1 expression inhibited the promoting effects of *circBART2.2* on T-cell apoptosis in HONE1 and HK1 after overexpression of *circBART2.2* by flow cytometry (**Fig. 3D**; Supplementary Fig. S3D). Based on these, we concluded *circBART2.2* inhibited T-cell function and mediated NPC immune escape through PD-L1.

## circBART2.2 bind to the helicase domain of RIG-I protein around nucleotides 114–165

To explore the molecular mechanisms through which *circBART2.2* affects PD-L1, RNA pulldown, followed by the mass spectrum identification, was performed in HONE1 using biotin-labeled *circBART2.2* (**Fig. 4A**). A total of 172 potential proteins were precipitated and identified (Supplementary Table S5). Then the GSE12452 GEO data set was used to analyze PD-L1 correlated genes. A total of 326 genes were positively correlated to PD-L1 expression ($r > 0.5$) while 247 genes were negatively correlated to PD-L1 ($r < -0.5$; Supplementary Fig. S4A). RIG-I (DDX58) was pulled down by *circBART2.2* and also positively correlated to PD-L1 expression. Both of RIG-I and PD-L1 genes were highly expressed and positively correlated with each other in GSE12452 (Supplementary Fig. S4B). IHC confirmed that RIG-I was highly expressed (**Fig. 4B**) and positively correlated with *circBART2.2* and PD-L1 protein expression in 52 NPC tissues, compared with that in 36 noncancerous samples (Supplementary Fig. S4C).

RNA pulldown experiments further confirmed biotin-labeled *circBART2.2* precipitated RIG-I protein in *circBART2.2*-overexpressing HONE1 and HK1 (**Fig. 4C**). RNA immunoprecipitation showed that anti-RIG-I–antibody-enriched exogenous *circBART2.2* in *circBART2.2*-overexpressing HONE1 and HK1 or endogenous *circBART2.2* in HONE1-EBV and HK1-EBV (**Fig. 4D**).

To explore the molecular mechanism underlying the promotion of RIG-I signaling by *circBART2.2, in vitro* RNA pulldown and RNA immunoprecipitation (RIP) assays were performed to determine the

(*Continued.*) ***, $P < 0.001$. **E,** The binding between *circBART2.2* and the helicase domain of RIG-I protein was detected in HONE1 and HK1 cells after cotransfection of the *circBART2.2* overexpression vector and the RIG-I full-length or truncated fragments using RNA pulldown assays with a biotin-labeled *circBART2.2* probe. **F,** The binding between *circBART2.2* and the helicase domain of RIG-I protein was examined in HONE1 and HK1 cells after the cotransfection of the *circBART2.2* overexpression vector and the Flag-tagged RIG-I full-length or truncated fragments by RNA immunoprecipitation using anti-Flag-RIG-I antibody. IgG was used as a control. **G,** The 114–165 nt of *circBART2.2* was crucial for the binding between *circBART2.2* and RIG-I proteins. HONE1 and HK1 cells were transfected with the full-length *circBART2.2* (WT) or deletion mutants (367–11 nt for DEL1, 62–89 nt for DEL2, 114–165 nt for DEL3). RNA pulldown assays were performed using a biotin-labeled *circBART2.2* probe, followed by Western blotting using anti–RIG-I antibody. Unbiotin-labeled *circBART2.2* or mutant probes were used as controls. **H,** RIG-I protein directly binds to the 114–165 nt of *circBART2.2* in HONE1 and HK1 cells. Cells were cotransfected with the FLAG-tagged RIG-I vector and the full-length *circBART2.2* (WT) or deletion mutants (DEL1, DEL2, and DEL3). RNA immunoprecipitation was performed using anti-Flag-RIG-I antibody, followed by qPCR analysis for *circBART2.2*. NS, not significant; ***, $P < 0.001$.

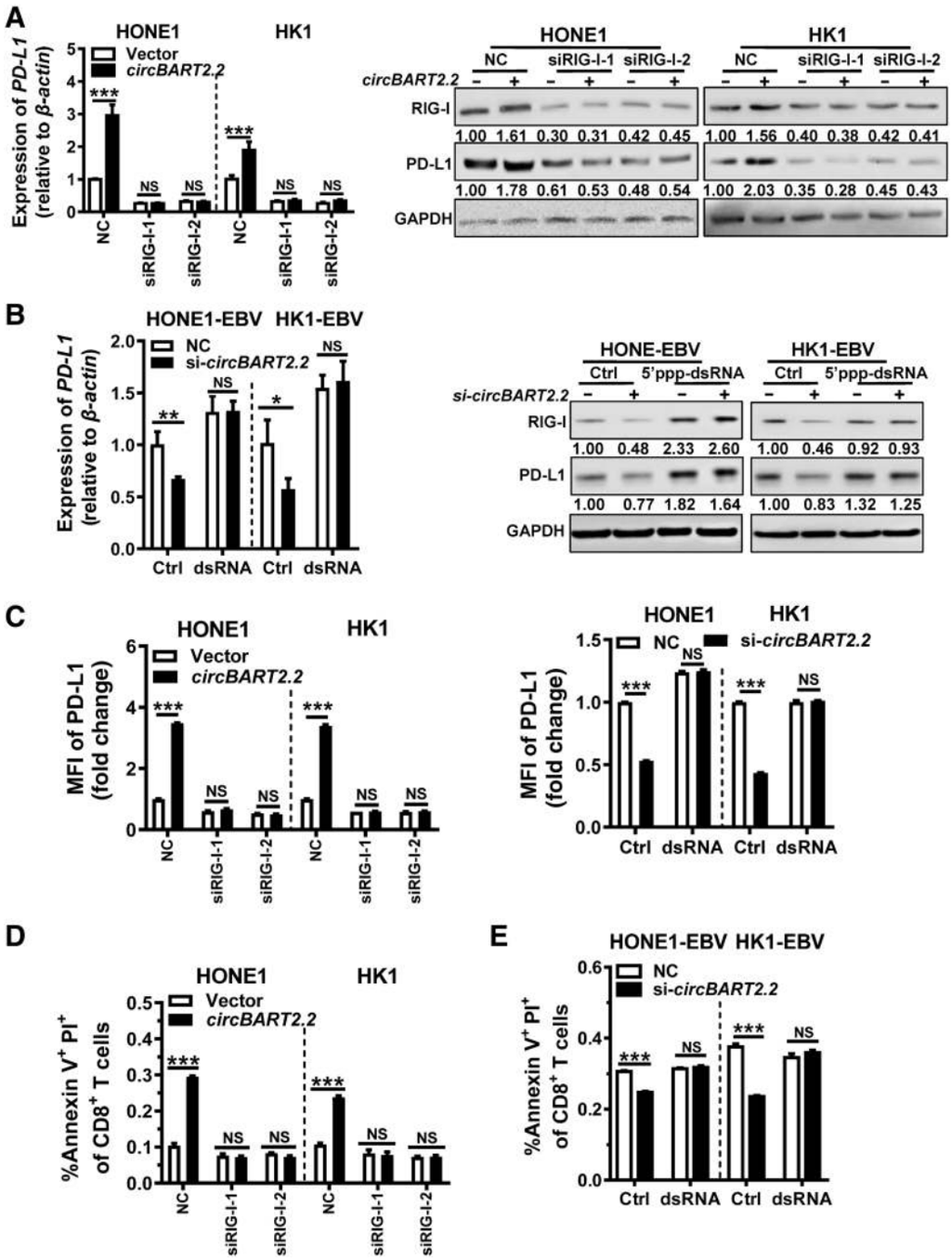


**Figure 5.**

*circBART2.2* regulates PD-L1 expression through binding to RIG-I. **A,** PD-L1 expression was examined in HONE1 and HK1 cells after *circBART2.2* overexpression or knockdown of RIG-I simultaneously using RT-PCR or Western blotting. **B,** PD-L1 expression was examined in HONE1-EBV and HK1-EBV cells after *circBART2.2* knockdown and RIG-I activator 5′-ppp-dsRNA treatment using RT-PCR or Western blotting. **C,** The expression of PD-L1 was measured in HONE1 and HK1 cells after *circBART2.2* overexpression and simultaneous RIG-I knockdown or HONE1-EBV and HK1-EBV cells after *circBART2.2* knockdown and simultaneous RIG-I activator 5′-ppp-dsRNA treatment by flow-cytometric analysis using anti–PD-L1 antibody. Each experiment was independently repeated three times; the original results are shown in Supplementary Fig. S6C. MFI, mean fluorescence intensity. **D,** Annexin $V^+$ $PI^+$ cells of CD8-positive active T cells were measured by flow cytometry in T cells cocultured with EBV-negative HONE1 and HK1cells after *circBART2.2* overexpression or knockdown of RIG-I simultaneously. Each experiment was independently repeated three times; the original results are shown in Supplementary Fig. S7B. **E,** Proportions of CD8-positive active T cells were measured by flow cytometry in T cells cocultured with HONE1-EBV and HK1-EBV cells after *circBART2.2* knockdown and simultaneous RIG-I activator 5′-ppp-dsRNA treatment. Each experiment was independently repeated three times; the original results are shown in Supplementary Fig. S7C. NS, not significant; ***, $P < 0.001$.

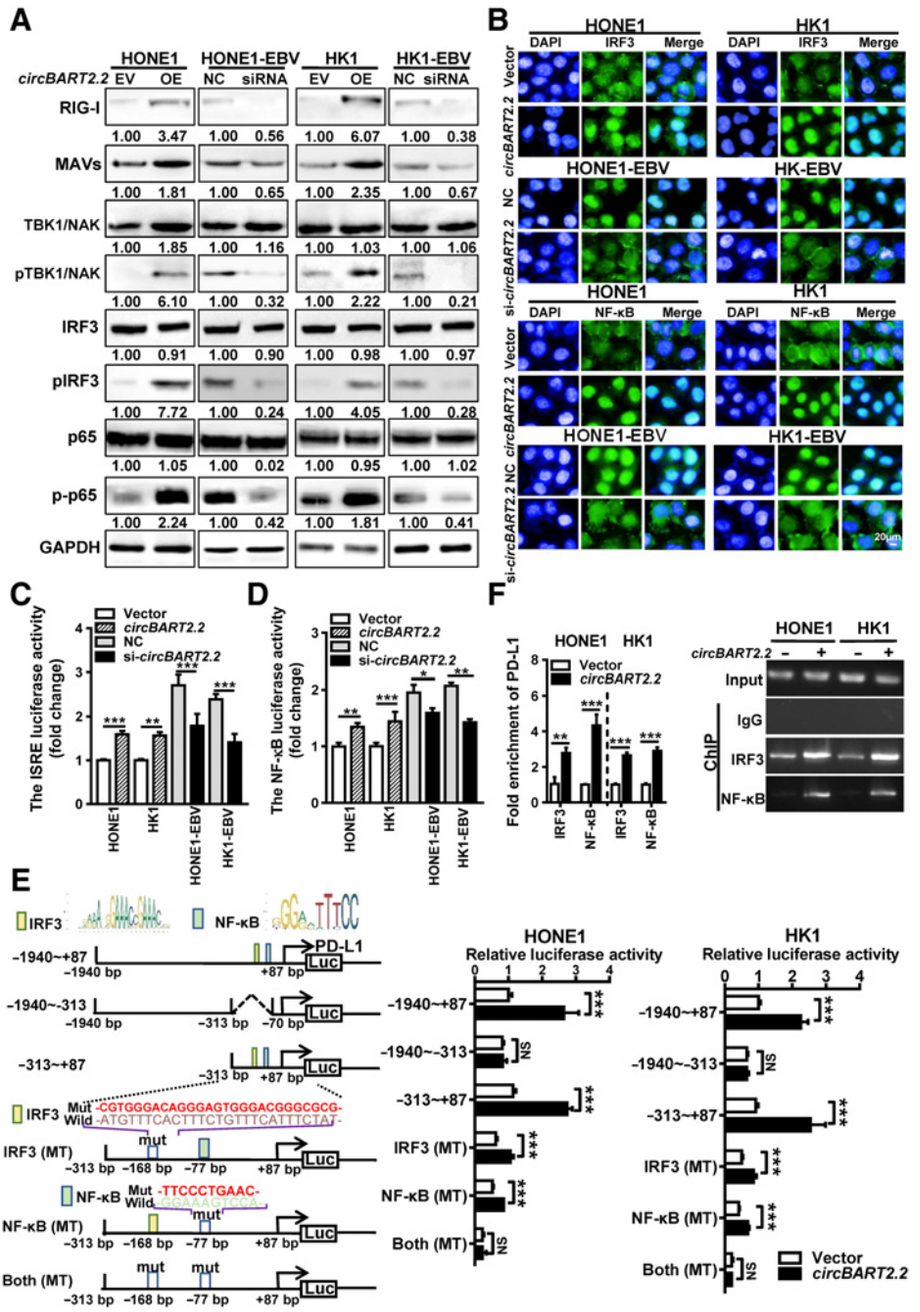


**Figure 6.**

*circBART2.2* upregulated PD-L1 expression by activating the transcriptional activity of IRF3 and NF-κB. **A,** The expression levels of RIG-I, MAVS, TBK1/NAK, IRF3, NF-κB (p65), phospho-TBK1/phospho-NAK, phospho-IRF3, and phospho-NF-KB (p-p65) were examined by Western blotting in HONE1 and HK1 cells after overexpression of *circBART2.2* or in HONE1-EBV and HK1-EBV cells after knockdown of *circBART2.2*. **B,** Immunofluorescence analysis was used to evaluate the nuclear entry of the transcription factors IRF3 or NF-κB (green) in HONE1 and HK1 cells after overexpression of *circBART2.2* or in HONE1-EBV and HK1-EBV cells after knockdown of *circBART2.2*. Nuclei were stained with DAPI (blue). Magnification, ×400. Scale bar, 50 μm. **C,** The transcriptional activity of IRF3 was measured using the IRSE luciferase reporter assays in HONE1 and HK1 cells after *circBART2.2* overexpression or in HONE1-EBV and HK1-EBV cells after *circBART2.2* knockdown. **, $P < 0.01$; ***, $P < 0.001$. **D,** The transcriptional activity of NF-κB was measured using the NF-κB luciferase reporter assays in HONE1 and HK1 cells after *circBART2.2* overexpression or in HONE1-EBV and HK1-EBV cells after *circBART2.2* knockdown. *, $P < 0.05$; **, $P < 0.01$; ***, $P < 0.001$. **E,** A series of luciferase reporter vectors was constructed according to the PD-L1 promoter sequence. Luciferase reporter activity was analyzed in HONE1 and HK1 cells after *circBART2.2* overexpression. The binding site of IRF3 transcription factor at −168 bp and NF-κB transcription factor at −77 bp on the PD-L1 promoter region were predicted according to the PD-L1 promoter (left); the results of luciferase reporters activity in HONE1 and HK1 cells after *circBART2.2* overexpression (right). ***, $P < 0.001$. **F,** Binding of the transcription factors IRF3 and NF-κB on the PD-L1 promoter region was detected by ChIP assays according to the predicted IRF3 and NF-κB binding sites. NS, not significant; **, $P < 0.001$; ***, $P < 0.001$. Left, the statistical results; right, the gel electrophoresis.

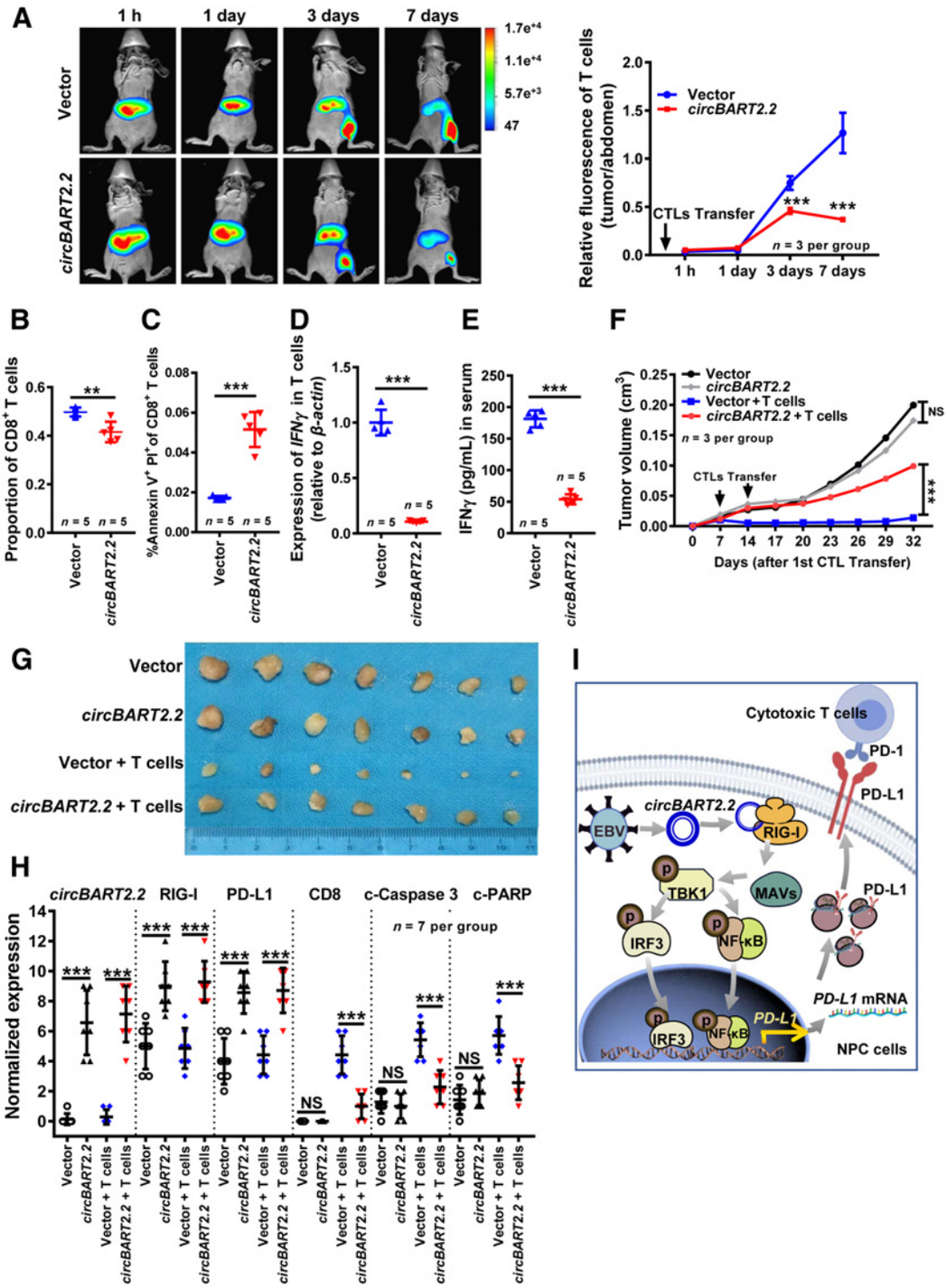


**Figure 7.**

*circBART2.2* induced NPC immune escape in nude mice. **A,** Living animal imaging analysis was used to detect the survival and distribution of human primary T cells in xenograft tumor mice ($n = 3$ per group) after injection of T cells. T cells were labeled with DeepRed. Left, representative images. Right, statistical results according to the DiR fluorescence signal ratio in mice collected at 1 day, 3 days, 5 days, and 7 days post injection (the DiR fluorescence signal ratio, T-cell fluorescence intensity in tumors of the root of the right thigh: T-cell fluorescence intensity in the abdomen of mice). The color scales indicate the DiR fluorescence intensity of T cells in mice. **B,** The proportion of $CD8^+$ T cells to all $CD3^+$ T cells was measured by flow cytometry using PE-Cy7–stained anti-CD8 antibody in human primary T cells of mice serum in HONE1 cell-derived xenograft mice models. A density of $5 \times 10^6$ HONE1 cells was transfected with the *circBART2.2* overexpression vector or the negative control (NC). Activated T cells were injected into nude mice, and after 14 days the peripheral blood was extracted for flow cytometry; $n = 5$ per group. **C,** Annexin $V^+$ $PI^+$ cells of CD8-positive T cells were measured by flow cytometry in HONE1 cell–derived xenograft mice models. (*Continued on the following page.*)

domain of RIG-I that binds to *circBART2.2*. *circBART2.2* binds to the helicase domain with RIG-I but not to the CARD domain in HONE1 and HK1 (**Fig. 4E** and **F**). Meanwhile, three well-characterized stem loop structures of *circBART2.2* (367–11 nt, 62–89 nt, and 114–165 nt) were predicted to bind with RIG-I protein (Supplementary Fig. S5A and S5B). RNA pulldown assay and RIP indicated the 114 to 165 nt region (DEL3) of *circBART2.2* was the critical region to bind to RIG-I in HONE1 and HK1 after overexpression of the *circBART2.2* WT vector or three truncated *circBART2.2* fragments (DEL1, DEL2, or DEL3; Supplementary Fig. S5C; **Fig. 4G** and **H**).

### circBART2.2 induced PD-L1–associated NPC immune escape by binding to RIG-I

To explore whether *circBART2.2* regulates PD-L1 by binding to RIG-I, RIG-I was knocked down in HONE1 and HK1 using two siRNAs or activated using 5′ppp-dsRNA (tlrl-3prna, Invitrogen) in HONE1-EBV and HK1-EBV (Supplementary Fig. S6A and S6B). qRT-PCR and Western blotting showed *circBART2.2* significantly upregulated PD-L1, whereas upregulation of PD-L1 by *circBART2.2* was inhibited by two siRIG-Is (**Fig. 5A**). Conversely, activation of RIG-I reversed the inhibition of PD-L1 by si-*circBART2.2* in HONE1-EBV and HK1-EBV (**Fig. 5B**). Flow cytometry (**Fig. 5C**; Supplementary Fig. S6C) and immunofluorescence (Supplementary Fig. S6D) also validated the above experimental results using an anti–PD-L1 antibody. These results suggested *circBART2.2* upregulated PD-L1 expression through binding with RIG-I protein.

To identify whether RIG-I affects the function of *circBART2.2* in T-cell apoptosis, HONE1 and HK1 were cotransfected with the *circBART2.2* overexpression vector and siRIG-I and then cocultured with activated human primary T cells. High-content cell imaging analysis showed knockdown of RIG-I inhibited the decrease in T-cell fluorescence intensity caused by *circBART2.2* (Supplementary Fig. S7A). Flow cytometry using anti-CD8 antibody showed the ability of *circBART2.2* to induce T-cell apoptosis was inhibited after knockdown of RIG-I. Conversely, the activation of RIG-I reversed the inhibitory effects of *circBART2.2* knockdown on T-cell apoptosis in HONE1-EBV and HK1-EBV (**Fig. 5D** and **E**; Supplementary Fig. S7B and S7C), suggesting that *circBART2.2* regulates T-cell apoptosis and tumor immune escape through the RIG-I signaling pathway.

### circBART2.2 upregulated PD-L1 by activating the transcription factors IRF3 and NF-κB

To explore whether *circBART2.2* regulates the RIG-I pathway, the expression of related molecules in the RIG-I pathway was detected by Western blotting in HONE1 and HK1 after overexpression of *circBART2.2* or in HONE1-EBV and HK1-EBV following knockdown of *circBART2.2*. Overexpression of *circBART2.2* increased the levels of RIG-I, mitochondrial antiviral-signaling protein (MAVS), TANK binding kinase 1 (TBK1)/NF-κB activating kinase (NAK), phospho-TBK1/phospho-NAK, phospho-IRF3, and phospho-NF-κB (p-p65), whereas knockdown of *circBART2.2* reduced the levels of these factors (**Fig. 6A**). *circBART2.2* significantly promoted the nuclear entry of transcription factors NF-κB and IRF3, whereas knockdown of *circBART2.2* decreased it by immunofluorescence (**Fig. 6B**). Luciferase reporter activity assays showed that overexpression of *circBART2.2* promoted the transcriptional activities of IRF3 and NF-κB in HONE1 and HK1, whereas knockdown of *circBART2.2* decreased the activities of them in HONE1-EBV and HK1-EBV (**Fig. 6C** and **D**).

To identify if *circBART2.2* regulates RIG-I expression at the transcription level, the *RIG-I* mRNA expression was also examined by qRT-PCR in HONE1 and HK1 or HONE1-EBV and HK1-EBV after *circBART2.2* overexpression or knockdown. *circBART2.2* significantly upregulated RIG-I expression at the mRNA level (Supplementary Fig. S8A). The Jaspar software showed there was a binding site of NF-κB near −342 bp of the RIG-I promoter. ChIP experiment confirmed that *circBART2.2* promoted the enrichment of NF-κB on the RIG-I promoter in HONE1 and HK1 (Supplementary Fig. S8B), suggesting that *circBART2.2* can also promote activation of RIG-I at the transcription level. Taken together, these results suggested that *circBART2.2* as an exogenous circRNA molecule encoded by EBV activated the RIG-I signaling pathway in NPC.

To further explore whether *circBART2.2* regulates PD-L1 through the RIG-I signaling pathway, transcription factor binding sites on the PD-L1 promoter were analyzed. Binding sites for IRF3 at −168 bp and for NF-κB at −77 bp were shown on the *PD-L1* promoter. Luciferase reporter activity revealed that the core promoter region of *PD-L1* was located from −313 to + 87 bp. Overexpression of *circBART2.2* increased the luciferase reporter activity at positions −313 to + 87 bp on the *PD-L1* promoter in HONE1 and HK1; however, this effect was blocked by mutation of the binding sites for IRF3 or NF-κB (**Fig. 6E**). ChIP experiments also showed that *circBART2.2* promoted the enrichment of IRF3 or NF-κB on the *PD-L1* promoter (**Fig. 6F**). Collectively, it is conceivable that the binding of *circBART2.2* to RIG-I results in PD-L1 upregulation through an IRF3- and NF-κB–initiated transcriptional program.

### circBART2.2 promoted immune escape of NPC cells *in vivo*

To test whether *circBART2.2* promotes the immune escape of NPC *in vivo*, HONE1 cells after overexpression of circBART2.2 were inoculated into nude mice to establish a xenograft model. As shown in Supplementary Fig. S9A, T cells were significantly aggregated toward the site of migrating tumors on day 3, and *circBART2.2* significantly decreased the fluorescence intensity of T cells at the site of migration tumors on day 7, suggesting that *circBART2.2* could promote T-cell apoptosis *in vivo*, leading to immune escape (**Fig. 7A**). Additionally, *circBART2.2* decreased the proportion of CD8-positive T cells among CD3-positive T cells and increased the proportion of apoptotic T cells by flow cytometry (**Fig. 7B** and **C**; Supplementary Fig. S9B and S9C). qRT-PCR (**Fig. 7D**) and ELISA (**Fig. 7E**) showed that *circBART2.2* inhibited the ability of T cells to secrete IFNγ in T cells and mice serum.

(*Continued.*) Mice peripheral blood was extracted for flow cytometry after incubation with PE-Cy7–stained anti-CD8 antibody, $n = 5$ per group. **D,** qRT-PCR analysis of *IFNγ* mRNA levels in peripheral blood after injection of activated T cells. *β-Actin* was used as an internal control; $n = 5$ per group. **E,** The IFNγ secretion in peripheral serum was detected by ELISA after injection of activated T cells; $n = 5$ per group. **F,** The tumor volumes for each group were measured after 32 days of tumor cells injection; $n = 7$ per group. ***, $P < 0.001$. **G,** The tumor images for each group were captured after 32 days of tumor cells injection; $n = 7$ per group. **H,** The statistical results for the expression of *circBART2.2*, RIG-I, PD-L1, CD8, cleaved caspase-3, and cleaved-PARP were analyzed using *in situ* hybridization or IHC in each mice tissue section. **, $P < 0.01$; ***, $P < 0.001$. **I,** Working model of *circBART2.2* promotes the RIG-I signaling pathway. In EBV-infected NPC cells, *circBART2.2* binds to the helicase domain of RIG-I protein through the binding sequence around 114 to 165 nt of *circBART2.2*, forming a complex to activate RIG-I. Activated RIG-I promotes PD-L1 transcription through its downstream transcription factors IRF3 and NF-κB, resulting in tumor immune escape in EBV-infected NPC cells. NS, not significant.

There were no significant differences in tumor size or body weight in nude mice between the *circBART2.2* group and the control group without T-cell injection; however, significant differences were observed in tumor volume, tumor size, tumor weight, and body weight between the *circBART2.2* group and the control group with T-cell injection (**Fig. 7F** and **G**; Supplementary Fig. S9D and S9E), suggesting that *circBART2.2* induced tumor immune escape in nude mice. IHC showed that RIG-I and PD-L1 were highly expressed in mice tumors in the *circBART2.2* group, regardless of whether T cells were injected. The numbers of CD8-positive T cells and apoptotic tumor cells [cleaved-caspase-3, cleaved-poly (ADP ribose) polymerase (PARP)] in the *circBART2.2* group injected with T cells were significantly lower than those in the control group injected with T cells (**Fig. 7H**; Supplementary Fig. S9F). These results underscore significance of RIG-I in the process of the *circBART2.2* -triggered tumor immune escape in promoting PD-L1 expression *in vivo*.

In this study, EBV-encoded *circBART2.2* was found to be highly expressed in NPC tissues and induced the upregulation of PD-L1 in NPC by binding with RIG-I protein to activate its signaling pathway, leading to immune escape in NPC. The binding sequence around 114–165 bp was crucial for the function of *circBART2.2*. *circBART2.2* interacts with the helicase domain of RIG-I, consequently strengthening RIG-I–mediated PD-L1 transcription and downstream signaling to initiate tumor immune escape in NPC (**Fig. 7I**).

## Discussion

EBV was the first virus shown to be associated with human tumors and closely related to the pathogenesis of NPC, gastric cancer, Burkitt lymphoma, and other tumors (32). Several proteins and miRNAs encoded by EBV are involved in tumor progression and malignant phenotypes (33, 34). EBV is also found to be one of the first viruses to encode circRNAs (17, 35). Among them, *circLMP2* was reported to induce stemness in EBV-associated gastric cancer cells (36). *circBART2.2* (EBV-*circRPMS1*) showed that it was expressed in EBV-positive cell lines and tissues representing latency types I, II, and III, including EBV-positive post-transplant lymphoproliferative disorder (PTLD), Burkitt lymphoma, EBV-associated gastric carcinoma, NPC, and AIDS-associated lymphoma (17, 36). Liu and colleagues found that *circBART2.2* was increased in metastatic NPC and was associated with a short survival time. However, the molecular mechanisms of *circBART2.2* still needs to be further clarified (25). In this study, we detected the high expression of *circBART2.2* in NPC clinical samples and cell lines. Although other EBV-encoded circRNAs were not detected or lowly expressed in EBV-positive NPC cells, they may be expressed in other EBV-associated cancer cells. The high expression of *circBART2.2* suggested that *circBART2.2* may play important biological roles in NPC.

EBV infection is closely related to tumor immune escape through upregulation of PD-L1 expression in various tumors (3, 37, 38). EBV-encoded *LMP1* (39), *EBNA2* (40), and *miR-BART5–5p* (41) have been reported to cooperate with PD-L1, affect T-cell immune recognition and clearance, and ultimately promote tumor immune escape (42). In this study, we made some preliminary exploration regarding the possible function of *circBART2.2*, which could bind with RIG-I to regulate PD-L1 and promote tumor immune escape, highlighting this new role of EBV infection in NPC.

RIG-I has generally been used as a key sensor of viral infection (43). Activation of RIG-I results in activation of PD-L1 through IRF3 and NF-kB transcription factors (28, 44–46). Exogenous circRNAs generally lead to activation of RIG-I (47, 48). In NPC, EBV infection is tightly associated with RIG-I–mediated inflammation (28, 49). EBV-encoded *EBER1* (50), *miR-BART6-3p* (30), and *LMP1* (29) regulate the activity of RIG-I in NPC. In this study, *circBART2.2*, as an exogenous circRNA of host cells, could bind with RIG-I protein to activate PD-L1 and promote tumor immune escape. Further studies are needed to determine whether *circBART2.2* can affect other biological phenotypes of NPC through RIG-I.

The siRNAs for *circBART2.2* were designed to span the circular splice sites of exons IV and IIIA of the BART gene, which is specific only to circular forms, and BART mRNA cannot be amplified. Theoretically, both *circBART2.1* and *circBART2.2* could be knocked down because they share the same back splice site. However, our data showed that only *circBART2.2* was highly expressed, and *circBART2.1* was not or very lowly expressed in NPC cells. Overexpression of *circBART2.1* in NPC did not regulate the expression of PD-L1. RNA pulldown and RIP assays showed that the 114 to 165 nt region (DEL3) of *circBART2.2* was the critical region to bind to RIG-I. This 114 to 165 nt region is unique to the *circBART2.2* sequence. Therefore, we speculate that *circBART2.1* may have little influence on the regulation of PD-L1 through the RIG-I pathway in NPC.

In conclusion, we identified the functions of *circBART2.2* in NPC immune escape for the first time. As an exogenous circRNA, *circBART2.2* promoted PD-L1 expression by binding to RIG-I protein and activating the RIG-I pathway, leading to the immune escape of NPC cells. The interplay between *circBART2.2* and RIG-I has important implications for EBV-associated NPC therapy. Targeting *circBART2.2* therapy generates a superior antitumor immune response that is critically dependent on PD-L1 expression, highlighting the role of *circBART2.2* in the antitumor immunity of EBV-infected NPC, which will help establish a novel approach to efficiently reprogram or restore protective antitumor immunity for NPC immunotherapy.

### Authors' Disclosures

No disclosures were reported.

### Authors' Contributions

**J. Ge:** Conceptualization, resources, data curation, software, formal analysis, visualization, methodology, writing–original draft. **J. Wang:** Resources, data curation, formal analysis. **F. Xiong:** Resources, data curation. **X. Jiang:** Resources, data curation. **K. Zhu:** Resources, data curation. **Y. Wang:** Software, formal analysis. **Y. Mo:** Resources, data curation. **Z. Gong:** Data curation. **S. Zhang:** Formal analysis. **Y. He:** Software, formal analysis. **X. Li:** Formal analysis. **L. Shi:** Formal analysis. **C. Guo:** Data curation. **F. Wang:** Data curation. **M. Zhou:** Formal analysis. **B. Xiang:** Data curation. **Y. Li:** Formal analysis, writing–original draft. **G. Li:** Formal analysis, writing–original draft. **W. Xiong:** Writing–original draft, writing–review and editing. **Z. Zeng:** Conceptualization, supervision, funding acquisition, validation, project administration, writing–review and editing.

### Acknowledgments

This work was supported in part by grants from the National Natural Science Foundation of China (81772928, 81803025, 81972776, and U20A20367) and the Natural Science Foundation of Hunan Province (2019JJ50872). The authors thank Professors George Sai Wah Tsao, Xin Li, and Lunquan Sun for providing EBV-positive cell lines.

The costs of publication of this article were defrayed in part by the payment of page charges. This article must therefore be hereby marked *advertisement* in accordance with 18 U.S.C. Section 1734 solely to indicate this fact.

Received December 28, 2020; revised May 2, 2021; accepted July 27, 2021; published first July 28, 2021.

## References


1. Jiang X, Wang J, Deng X, Xiong F, Ge J, Xiang B, et al. Role of the tumor microenvironment in PD-L1/PD-1-mediated tumor immune escape. Mol Cancer 2019;18:10.
2. Ren D, Hua Y, Yu B, Ye X, He Z, Li C, et al. Predictive biomarkers and mechanisms underlying resistance to PD1/PD-L1 blockade cancer immunotherapy. Mol Cancer 2020;19:19.
3. Ma BBY, Lim WT, Goh BC, Hui EP, Lo KW, Pettinger A, et al. Antitumor activity of nivolumab in recurrent and metastatic nasopharyngeal carcinoma: an international, multicenter study of the mayo clinic phase 2 consortium (NCI-9742). J Clin Oncol 2018;36:1412–8.
4. Sun C, Mezzadra R, Schumacher TN. Regulation and function of the PD-L1 checkpoint. Immunity 2018;48:434–52.
5. Fan C, Zhang S, Gong Z, Li X, Xiang B, Deng H, et al. Emerging role of metabolic reprogramming in tumor immune evasion and immunotherapy. Sci China Life Sci 2021;64:534–47.
6. Wei F, Wang D, Wei J, Tang N, Tang L, Xiong F, et al. Metabolic crosstalk in the tumor microenvironment regulates antitumor immunosuppression and immunotherapy resisitance. Cell Mol Life Sci 2021;78:173–93.
7. Wu C, Li M, Meng H, Liu Y, Niu W, Zhou Y, et al. Analysis of status and countermeasures of cancer incidence and mortality in China. Sci China Life Sci 2019;62:640–7.
8. Tang T, Yang L, Cao Y, Wang M, Zhang S, Gong Z, et al. LncRNA AATBC regulates Pinin to promote metastasis in nasopharyngeal carcinoma. Mol Oncol 2020;14:2251–70.
9. Tu C, Zeng Z, Qi P, Li X, Guo C, Xiong F, et al. Identification of genomic alterations in nasopharyngeal carcinoma and nasopharyngeal carcinoma-derived Epstein-Barr virus by whole-genome sequencing. Carcinogenesis 2018;39:1517–28.
10. Tu C, Zeng Z, Qi P, Li X, Yu Z, Guo C, et al. Genome-wide analysis of 18 Epstein-Barr viruses isolated from primary nasopharyngeal carcinoma biopsy specimens. J Virol 2017;91:e00301–17.
11. Xiong F, Deng S, Huang HB, Li XY, Zhang WL, Liao QJ, et al. Effects and mechanisms of innate immune molecules on inhibiting nasopharyngeal carcinoma. Chin Med J 2019;132:749–52.
12. Wu Y, Wei F, Tang L, Liao Q, Wang H, Shi L, et al. Herpesvirus acts with the cytoskeleton and promotes cancer progression. J Cancer 2019;10:2185–93.
13. Zhao J, Guo C, Xiong F, Yu J, Ge J, Wang H, et al. Single cell RNA-seq reveals the landscape of tumor and infiltrating immune cells in nasopharyngeal carcinoma. Cancer Lett 2020;477:131–43.
14. Wu Y, Wang D, Wei F, Xiong F, Zhang S, Gong Z, et al. EBV-miR-BART12 accelerates migration and invasion in EBV-associated cancer cells by targeting tubulin polymerization-promoting protein 1. FASEB J 2020;34:16205–23.
15. Wang D, Zeng Z, Zhang S, Xiong F, He B, Wu Y, et al. Epstein-Barr virus-encoded miR-BART6-3p inhibits cancer cell proliferation through the LOC553103-STMN1 axis. FASEB J 2020;34:8012–27.
16. He B, Li W, Wu Y, Wei F, Gong Z, Bo H, et al. Epstein-Barr virus-encoded miR-BART6-3p inhibits cancer cell metastasis and invasion by targeting long noncoding RNA LOC553103. Cell Death Dis 2016;7:e2353.
17. Toptan T, Abere B, Nalesnik MA, Swerdlow SH, Ranganathan S, Lee N, et al. Circular DNA tumor viruses make circular RNAs. Proc Natl Acad Sci U S A 2018;115:E8737–E45.
18. Li P, Zhu K, Mo Y, Deng X, Jiang X, Shi L, et al. Research progress of circRNAs in head and neck cancers. Front Oncol 2021;11:616202.
19. Wang Y, Mo Y, Peng M, Zhang S, Gong Z, Yan Q, et al. The influence of circular RNAs on autophagy and disease progression. Autophagy 2021:1–14.
20. Fan CM, Wang JP, Tang YY, Zhao J, He SY, Xiong F, et al. circMAN1A2 could serve as a novel serum biomarker for malignant tumors. Cancer Sci 2019;110:2180–8.
21. Wu P, Mo Y, Peng M, Tang T, Zhong Y, Deng X, et al. Emerging role of tumor-related functional peptides encoded by lncRNA and circRNA. Mol Cancer 2020;19:22.
22. Zhong Y, Du Y, Yang X, Mo Y, Fan C, Xiong F, et al. Circular RNAs function as ceRNAs to regulate and control human cancer progression. Mol Cancer 2018;17:79.
23. Fan C, Qu H, Xiong F, Tang Y, Tang T, Zhang L, et al. CircARHGAP12 promotes nasopharyngeal carcinoma migration and invasion via ezrin-mediated cytoskeletal remodeling. Cancer Lett 2021;496:41–56.
24. Tang L, Xiong W, Zhang L, Wang D, Wang Y, Wu Y, et al. circSETD3 regulates MAPRE1 through miR-615-5p and miR-1538 sponges to promote migration and invasion in nasopharyngeal carcinoma. Oncogene 2021;40:307–21.
25. Liu Q, Shuai M, Xia Y. Knockdown of EBV-encoded circRNA circRPMS1 suppresses nasopharyngeal carcinoma cell proliferation and metastasis through sponging multiple miRNAs. Cancer Manag Res 2019;11:8023–31.
26. Huang JT, Chen JN, Gong LP, Bi YH, Liang J, Zhou L, et al. Identification of virus-encoded circular RNA. Virology 2019;529:144–51.
27. Nahand JS, Jamshidi S, Hamblin MR, Mahjoubin-Tehran M, Vosough M, Jamali M, et al. Circular RNAs: new epigenetic signatures in viral infections. Front Microbiol 2020;11:1853.
28. Duan Y, Li Z, Cheng S, Chen Y, Zhang L, He J, et al. Nasopharyngeal carcinoma progression is mediated by EBER-triggered inflammation via the RIG-I pathway. Cancer Lett 2015;361:67–74.
29. Xu C, Sun L, Liu W, Duan Z. Latent membrane protein 1 of Epstein-Barr virus promotes RIG-I degradation mediated by proteasome pathway. Front Immunol 2018;9:1446.
30. Lu Y, Qin Z, Wang J, Zheng X, Lu J, Zhang X, et al. Epstein-Barr virus miR-BART6-3p inhibits the RIG-I pathway. J Innate Immun 2017;9:574–86.
31. Cai L, Ye Y, Jiang Q, Chen Y, Lyu X, Li J, et al. Epstein-Barr virus-encoded microRNA BART1 induces tumour metastasis by regulating PTEN-dependent pathways in nasopharyngeal carcinoma. Nat Commun 2015;6:7353.
32. Fan C, Tang Y, Wang J, Xiong F, Guo C, Wang Y, et al. The emerging role of Epstein-Barr virus encoded microRNAs in nasopharyngeal carcinoma. J Cancer 2018;9:2852–64.
33. Pfeffer S, Sewer A, Lagos-Quintana M, Sheridan R, Sander C, Grasser FA, et al. Identification of microRNAs of the herpesvirus family. Nat Methods 2005;2:269–76.
34. Pfeffer S, Zavolan M, Grasser FA, Chien M, Russo JJ, Ju J, et al. Identification of virus-encoded microRNAs. Science 2004;304:734–6.
35. Ungerleider N, Concha M, Lin Z, Roberts C, Wang X, Cao S, et al. The Epstein Barr virus circRNAome. PLoS Pathog 2018;14:e1007206.
36. Gong LP, Chen JN, Dong M, Xiao ZD, Feng ZY, Pan YH, et al. Epstein-Barr virus-derived circular RNA LMP2A induces stemness in EBV-associated gastric cancer. EMBO Rep 2020;21:e49689.
37. Thompson ED, Zahurak M, Murphy A, Cornish T, Cuka N, Abdelfatah E, et al. Patterns of PD-L1 expression and CD8 T cell infiltration in gastric adenocarcinomas and associated immune stroma. Gut 2017;66:794–801.
38. Carbone A, Gloghini A, Carlo-Stella C. Are EBV-related and EBV-unrelated Hodgkin lymphomas different with regard to susceptibility to checkpoint blockade? Blood 2018;132:17–22.
39. Bi XW, Wang H, Zhang WW, Wang JH, Liu WJ, Xia ZJ, et al. PD-L1 is upregulated by EBV-driven LMP1 through NF-kappaB pathway and correlates with poor prognosis in natural killer/T-cell lymphoma. J Hematol Oncol 2016;9:109.
40. Anastasiadou E, Stroopinsky D, Alimperti S, Jiao AL, Pyzer AR, Cippitelli C, et al. Epstein-Barr virus-encoded EBNA2 alters immune checkpoint PD-L1 expression by downregulating miR-34a in B-cell lymphomas. Leukemia 2019;33:132–47.
41. Yoon CJ, Chang MS, Kim DH, Kim W, Koo BK, Yun SC, et al. Epstein-Barr virus-encoded miR-BART5-5p upregulates PD-L1 through PIAS3/pSTAT3 modulation, worsening clinical outcomes of PD-L1-positive gastric carcinomas. Gastric Cancer 2020;23:780–95.
42. Goodman A, Patel SP, Kurzrock R. PD-1-PD-L1 immune-checkpoint blockade in B-cell lymphomas. Nat Rev Clin Oncol 2017;14:203–20.
43. Jiang M, Zhang S, Yang Z, Lin H, Zhu J, Liu L, et al. Self-recognition of an inducible host lncRNA by RIG-I feedback restricts innate immune response. Cell 2018;173:906–19.
44. Antonangeli F, Natalini A, Garassino MC, Sica A, Santoni A, Di Rosa F. Regulation of PD-L1 expression by NF-kappaB in cancer. Front Immunol 2020;11:584626.
45. Ritprajak P, Azuma M. Intrinsic and extrinsic control of expression of the immunoregulatory molecule PD-L1 in epithelial cells and squamous cell carcinoma. Oral Oncol 2015;51:221–8.
46. Wang W, Chapman NM, Zhang B, Li M, Fan M, Laribee RN, et al. Upregulation of PD-L1 via HMGB1-activated IRF3 and NF-kappaB contributes to UV radiation-induced immune suppression. Cancer Res 2019;79:2909–22.

47. Chen YG, Chen R, Ahmad S, Verma R, Kasturi SP, Amaya L, et al. N6-methyladenosine modification controls circular RNA immunity. Mol Cell 2019;76:96–109.
48. Chen YG, Kim MV, Chen X, Batista PJ, Aoyama S, Wilusz JE, et al. Sensing self and foreign circular RNAs by intron identity. Mol Cell 2017; 67:228–38.
49. Jangra S, Yuen KS, Botelho MG, Jin DY. Epstein-Barr virus and innate immunity: friends or foes? Microorganisms 2019;7:183.
50. Cheng S, Li Z, He J, Fu S, Duan Y, Zhou Q, et al. Epstein-Barr virus noncoding RNAs from the extracellular vesicles of nasopharyngeal carcinoma (NPC) cells promote angiogenesis via TLR3/RIG-I-mediated VCAM-1 expression. Biochim Biophys Acta Mol Basis Dis 2019;1865:1201–13.